Research Square

Preprints are preliminary reports that have not undergone peer review.
They should not be considered conclusive, used to inform clinical practice,
or referenced by the media as validated information.

Reciprocal neutrophil–endothelial progenitor cell interactions regulate vascular injury in acute graft-versus-host disease

Xi Zhang

zhangxi@tmmu.edu.cn

Xinqiao Hospital

Qingxiao Song

Xinqiao Hospital

Yixiao Kang

Xinqiao Hospital

Xiaodong Xie

Xinqiao Hospital

Rui Wang

Xinqiao Hospital

Fengjuan Tian

Xinqiao Hospital

Research Article

Keywords: Acute graft-versus-host disease, Endothelial progenitor cells, Neutrophils, Vascular injury, RIPK1.

Posted Date: November 26th, 2026

DOI: https://doi.org/10.21203/rs.3.rs-11785954/v1

License: This work is licensed under a Creative Commons Attribution 4.0 International License.
Read Full License

Additional Declarations: No competing interests reported.

Reciprocal neutrophil–endothelial progenitor cell interactions regulate vascular injury in acute graft-versus-host disease

Authors: Yixiao Kang,[1-3#] Xiaodong Xie,[1-3#] Rui Wang,[1-4] Fengjuan Tian,[1-3] Qingxiao Song, [1-4*] Xi Zhang [1-4*]

Affiliations:

1. Medical Center of Hematology, Institute of Science Innovation for Blood Ecology and Intelligent Cells, Xinqiao Hospital, Army Medical University, Chongqing 400037, China.
2. Chongqing Key Laboratory of Hematology and Microenvironment, Xinqiao Hospital, Army Medical University, Chongqing 400037, China.
3. State Key Laboratory of Trauma and Chemical Poisoning, Army Medical University, Chongqing 400037, China.
4. Jinfeng Laboratory, Chongqing 401329, China.

*Corresponding authors:

Xi Zhang, E-mail: zhangxxi@sina.com, zhangxi@tmmu.edu.cn

Qingxiao Song, E-mail: qingxiaosong3@gmail.com

#Yixiao Kang and Xiaodong Xie contributed equally

Abstract

Background

Endothelial injury contributes to acute graft-versus-host disease (aGVHD), but how inflammation impairs endogenous vascular repair remains unclear. We investigated interactions between neutrophils and endothelial progenitor cells (EPCs) in the setting of murine aGVHD.

Methods

Murine aGVHD was established by transplantation from C57BL/6 donors into BALB/c recipients. Vascular injury was assessed by transmission electron microscopy, immunofluorescence staining, three-dimensional vascular imaging, and Evans blue extravasation. EPC apoptosis and neutrophil reactive oxygen species (ROS) levels were measured by flow cytometry. EPC viability was assessed using the CCK-8 assay. EPC function was evaluated using adhesion, migration, and tube formation assays. Neutrophil extracellular traps (NETs) formation was assessed by immunofluorescence staining. Neutrophil-EPC interactions were examined using direct and Transwell coculture. RIPK1 and phosphorylated MLKL protein levels were examined by immunoblotting. The therapeutic effects of the RIPK1 inhibitor ORIC-559 and EPC administration were evaluated in vivo. The graft-versus-leukemia (GVL) activity was assessed by bioluminescence imaging in BALB/c recipients transplanted with C57BL/6 donor cells and luciferase-expressing A20 B-cell lymphoma cells.

Results

aGVHD was characterized by vascular leakage and organ-specific vascular remodeling, accompanied by increased EPC oxidative stress and apoptosis and impaired EPC function. After transplantation, neutrophils infiltrating the liver and colon exhibited increased ROS levels, while bone marrow neutrophils showed enhanced NETs formation. Coculture with neutrophils from aGVHD recipients increased EPC apoptosis and reduced CCK-8 activity; this reduction was attenuated by degradation of extracellular DNA with DNase I. EPCs from aGVHD recipients

exhibited increased RIPK1 and phosphorylated MLKL protein levels. Treatment with the RIPK1 inhibitor ORIC-559 improved EPC survival, reduced vascular leakage, and attenuated aGVHD in vivo. Conversely, ex vivo-expanded EPCs suppressed neutrophil ROS levels in direct and Transwell coculture and reduced NETs formation. In vivo EPC administration reduced endothelial injury and neutrophil-associated inflammation and ameliorated aGVHD while preserving GVL activity.

Conclusions

These findings identify reciprocal interactions between neutrophils and EPCs that link innate inflammation to impaired vascular repair. They support the potential clinical translation of EPC-based therapy and RIPK1 inhibition in aGVHD.

Keywords

Acute graft-versus-host disease; Endothelial progenitor cells; Neutrophils; Vascular injury; RIPK1.

Introduction

Acute graft-versus-host disease (aGVHD) remains a major cause of morbidity and mortality after allogeneic hematopoietic stem cell transplantation (allo-HSCT) [1,2]. Antigen presenting cells (APCs) and T cells activation are central to aGVHD pathogenesis and drive tissue injury in the gastrointestinal (GI) tract, liver, and skin [3-5]. In addition to immune cell-mediated cytotoxicity, endothelial injury and dysfunction have been increasingly implicated in the pathogenesis of aGVHD [6,7]. The vascular endothelial cells (ECs) are critical interface between circulating immune cells and recipient tissues during allo-HSCT [8]. ECs regulate leukocyte trafficking and maintain vascular barrier integrity [7]. Clinical evaluation of endothelial dysfunction, including serum levels of angiopoietin-2 and soluble thrombomodulin, as well as endothelial activation and stress index (EASIX), are associated with GVHD severity and adverse transplant outcomes [6,9-12]. ECs also contribute to tissue tolerance after allo-HSCT, recent studies showed that IFNγ–IRF1 signaling in lymphatic ECs induces MHC II and PD-L1 and supports regulatory T cells (Tregs) expansion [13-15].

Endothelial progenitor cells (EPCs) regulate vascular repair by promoting ECs regeneration, neovascularization, and restoration of vascular integrity after injury [16]. EPCs also exert immunomodulatory effects through paracrine mediators, extracellular vesicles, and interactions with immune cells [16]. In patients with aGVHD, circulating and bone marrow-derived EPCs are reduced and exhibit impaired migratory and angiogenic capacity, increased oxidative stress, and enhanced apoptosis, with the extent of EPCs dysfunction associated with disease severity [17]. Previous studies have shown that EPCs administration can attenuate GVHD through vascular repair and modulation of T cell infiltration and Tregs expansion [18]. The mechanisms underlying EPCs injury during aGVHD and the contribution of innate immune cells to this process are not well defined.

Neutrophils rapidly reconstitute after allo-HSCT and mediate tissue inflammation in aGVHD. Neutrophils are recruited to sites of intestinal injury following conditioning and migrate to mesenteric lymph nodes, where they can promote donor T cells activation [19]. In addition, neutrophils also induce tissue injury through the production of reactive oxygen species (ROS) and the formation of neutrophil extracellular traps (NETs) [19-22]. Recent studies further demonstrate functional heterogeneity among graft-derived neutrophil populations, with distinct subsets associated with subsequent aGVHD risk [23]. However, whether neutrophils mediated vascular and EPCs injury in aGVHD remains unclear.

Here, we identify a reciprocal interaction between donor-derived neutrophils and EPCs that contributes to vascular injury in aGVHD. Activated donor neutrophils induce EPCs injury, whereas EPCs restrain neutrophil ROS production and NETs formation. Therapeutically, EPCs administration restores vascular integrity and attenuates aGVHD while preserving GVL activity, whereas pharmacologic inhibition of RIPK1 protects EPCs and similarly reduces disease severity. These findings provide a rationale for targeting both vascular repair and RIPK1 signaling as novel strategies to mitigate aGVHD.

Methods

Mice

BALB/c (H-2d) and C57BL/6J (H-2b) mice were purchased from Vital River Laboratory Animal Technology (Beijing, China). Male BALB/c mice aged 8 to 12 weeks were used as transplant recipients, and C57BL/6J mice aged 4 to 6 weeks were used for isolation of endothelial progenitor cells (EPCs). Mice were maintained under specific pathogen-free conditions at the

Jinfeng Laboratory. All animal procedures were performed in accordance with protocols approved by the Institutional Animal Care and Use Committee of Army Medical University (#AMUWEC20245225).

Murine aGVHD and GVL models

Male BALB/c recipients aged 8 to 12 weeks received lethal total-body irradiation (7.5 Gy) in 2 fractions on days −1 and 0. Six to eight hours after the second irradiation, recipients were injected intravenously with 5×10^6 bone marrow cells and 1.25×10^6 splenocytes from C57BL/6 donors. Syngeneic BALB/c to BALB/c transplantation was used as the non-GVHD control.

For GVL experiments, lethally irradiated BALB/c recipients received 5×10^6 T cell-depleted bone marrow cells (TCD-BM) and 1.25×10^6 splenocytes from C57BL/6 donors together with 5×10^6 luciferase- and GFP-expressing A20 cells (ZQXZbio, Shanghai, China). T cells were depleted from bone marrow using CD90.2 MicroBeads (Miltenyi Biotec, Germany), depletion efficiency was confirmed by flow cytometry and exceeded 95%.

Isolation, culture, and characterization of murine EPCs

EPCs were isolated from the femurs and tibias of wild type C57BL/6J mice. Bone marrow cells were flushed with phosphate-buffered saline (PBS), and mononuclear cells were isolated by Ficoll density-gradient centrifugation (Cytiva, United Kingdom). Cells were plated on fibronectin-coated culture dishes (Sigma-Aldrich, Germany) and maintained in complete EGM-2 medium (Lonza, Switzerland) supplemented with 50 mg/l murine vascular endothelial growth factor (VEGF; PeproTech, USA) at 37°C in 5% CO_2. After 48 hours, nonadherent cells were removed and fresh medium was added. Adherent cells were subsequently maintained with medium changes every 3 days and passaged at 80% to 90% confluence. After the first passage,

EPCs were characterized by flow cytometry and assessed for their capacity to form capillary-like networks before use in subsequent in vitro experiments or adoptive transfer.

Assessment of aGVHD severity and GVL activity

Clinical aGVHD severity was assessed using a previously described scoring system [24]. Histopathologic injury was evaluated in the liver, small intestine, and colon. Mice were anesthetized with isoflurane and euthanized by cervical dislocation, and tissues were collected, sectioned, and stained with hematoxylin and eosin (H&E). Histopathologic scoring was performed as previously described [25]. Briefly, hepatic GVHD was scored according to the extent of lymphocytic infiltration, tissue involvement, and hepatocellular necrosis, with a maximum score of 9. Intestinal GVHD was scored according to mononuclear cell infiltration and morphologic tissue injury, with a maximum score of 8. GVL activity was assessed by serial bioluminescence imaging using an AniView 600 in vivo imaging system (BLT, China) under isoflurane anesthesia. Tumor burden was quantified from bioluminescence signals as indicated.

Tissue 3D imaging

Mice were transcardially perfused with PBS and 4% PFA. Liver, bone marrow (flushed from femurs/tibiae; bone fragments decalcified if present), and colon (luminal contents flushed) were collected, post-fixed, washed, and sectioned at 500 μm. Labeled samples were cleared using the FDISCO reagent kit (JA11012, Jarvis (Wuhan) Biological Pharmaceutical Co., Ltd., China) according to the kit instructions: incubation in reagents A–E for 1 h each, followed by reagent F until transparent, all at 6–8 °C with slight shaking; incubation times were extended for thicker samples. Cleared samples were mounted between two cover glasses and imaged with an inverted confocal fluorescence microscope (LSM880, Zeiss, Germany) using a Fluar 63×/1.4 oil objective (working distance, 0.2 mm). Images were processed with Zen (Zeiss, Germany) and reconstructed

with Imaris 10.1 software. Images were analyzed using Imaris (Filament Tracer) for 3D reconstruction and branch level color-coding (green, low; red, high), and whole-specimen parameters (VVD, VLD, and branch density) were quantified.

Evans blue vascular permeability assay

Vascular permeability was assessed using Evans blue extravasation as previously described [26]. Mice received 0.5% Evans blue in PBS (5 μl/g body weight; Sigma-Aldrich, Germany) by tail-vein injection. One hour later, mice were anesthetized and euthanized, followed by cardiac perfusion with PBS. Target tissues were collected, weighed, and incubated in formamide at 56°C for 24 hours in the dark. After centrifugation, absorbance of the supernatant was measured at 620 nm. Evans blue extravasation was expressed as micrograms of Evans blue per gram of wet tissue.

Apoptosis assay

Cell apoptosis was assessed using Alexa Fluor 647 Annexin V (BD Pharmingen; BD Biosciences, San Jose, CA) according to the manufacturer's instructions. Annexin V staining was quantified by flow cytometry.

Cell proliferation and viability assay

EPC proliferation was assessed using the Cell Counting Kit-8 (CCK-8; Dojindo Molecular Technologies, Japan) according to the manufacturer’s instructions. EPCs, either cultured alone or co-cultured with neutrophils were seeded in 96-well plates in 100 μl per well. CCK-8 reagent was added, and cells were incubated for 1 hour at 37°C. Absorbance at 450 nm was measured using a microplate reader (Thermo Scientific, USA).

EPC migration assay

EPC migration was assessed using 24-well Transwell chambers (Corning, USA). EPCs (1.5×10^5) were resuspended in serum-free medium and added to the upper chamber, with complete medium containing 10% fetal bovine serum (FBS) added to the lower chamber. After incubation for 12 hours at 37°C in 5% CO_2, membranes were washed with PBS and fixed with 4% paraformaldehyde. Nonmigrated cells were removed from the upper surface of the membrane, and migrated cells were stained with crystal violet (Biosharp, China) and imaged by light microscopy.

EPC adhesion assay

EPC adhesion was assessed by seeding 5×10^4 cells into 96-well plates precoated with fibronectin (50 μg/ml). After incubation for 40 minutes at 37°C, wells were washed 3 times with PBS to remove nonadherent cells. Adherent cells were stained with crystal violet (Biosharp, China) and imaged by light microscopy.

Measurement of intracellular ROS

Intracellular reactive oxygen species (ROS) were measured using 2′,7′-dichlorodihydrofluorescein diacetate (DCFH-DA; MedChemExpress, USA). Fluorescence intensity was quantified by flow cytometry.

EPC and neutrophil coculture

Bone marrow cells were flushed from the femurs and tibias with PBS, and neutrophils were enriched using a mouse Neutrophil Isolation Kit (Miltenyi Biotec, Germany). Two EPC-neutrophil coculture systems were used. In the first, neutrophils and EPCs were cultured at a 1:1 ratio in RPMI 1640 containing 10% FBS for 4 hours. For contact-independent coculture, the 2 cell populations were separated using Transwell inserts with 0.4-μm pores. In the second system,

neutrophils and EPCs were cultured at a 20:1 ratio in RPMI 1640 containing 2% FBS for 6 hours. Cells and culture supernatants were collected at the indicated time points for subsequent analyses.

Transmission electron microscopy

Freshly harvested tissues were cut into approximately 1-mm^3 pieces and immediately fixed in 2.5% glutaraldehyde at 4°C. Samples were washed in 0.1 M phosphate buffer, postfixed in 1% osmium tetroxide, dehydrated through a graded ethanol series, and embedded in epoxy resin. Ultrathin sections (70 nm) were stained with uranyl acetate and lead citrate and examined by transmission electron microscopy.

Immunofluorescence staining

Paraffin-embedded tissue sections or primary cultured cells were fixed with 4% paraformaldehyde for 15 minutes and permeabilized with 0.1% Triton X-100. Samples were blocked with 1% goat serum at room temperature and incubated overnight at 4°C with primary antibodies against citrullinated histone H3 (CitH3; ab5103), Ly6G (ab25377), CD31 (ab222783), ZO-1 (ab221547), or α-smooth muscle actin (α-SMA; ab7817; all from Abcam, USA). Samples were then incubated with fluorophore-conjugated secondary antibodies for 1 hour at room temperature. Nuclei were counterstained with 4′,6-diamidino-2-phenylindole (DAPI; Solarbio, Beijing, China), and images were acquired using a Leica SP8 confocal microscope (Leica Microsystems, Wetzlar, Germany).

Immunol blotting

Cells were lysed in RIPA buffer containing protease inhibitors (Beyotime, Shanghai, China), and protein concentrations were determined using a bicinchoninic acid assay (Beyotime). Equal amounts of protein were separated by 10% SDS-polyacrylamide gel electrophoresis and

transferred to polyvinylidene difluoride membranes. Membranes were blocked with 5% bovine serum albumin and incubated overnight at 4°C with antibodies against RIPK1 (Proteintech, China), phosphorylated MLKL (Cell Signaling Technology, USA), or GAPDH (Cell Signaling Technology). After washing, membranes were incubated with horseradish peroxidase–conjugated goat anti-rabbit or goat anti-mouse secondary antibodies (Invitrogen, Carlsbad, CA). Protein bands were detected using an enhanced chemiluminescence substrate (Millipore, MA).

In vitro tube formation assay

The angiogenic capacity of EPCs was assessed by an in vitro tube formation assay. Pretreated EPCs were seeded onto Matrigel (Corning, USA) and capillary-like network formation was assessed at the indicated time points.

Antibodies and flow cytometry

Monoclonal antibodies against mouse TCR-β (H57-597), TNF-α (MP6-XT22), pro-IL-1β(NJTEN3), CD309 (Avas12a1), Sca-1 (D7) were purchased from Thermo Fisher Scientific.The following mAbs against mouse H2Kb (AF6-88.5), Ly6G (1A8), CD11b (M1/70), CD34 (RAM34), CD31 (MEC 13.3), CD45 (30-F11), CD8 (53-6.7), IFN-γ (XMG1.2) were purchased from BD. Cell-surface and intracellular staining were performed according to the manufacturers' protocols. Samples were acquired using a BD LSRFortessa flow cytometer (BD Biosciences, Franklin Lakes, NJ), and data were analyzed using FlowJo version 11 (Tree Star, Ashland, OR).

Isolation of hepatic endothelial cells

Hepatic endothelial cells were isolated as previously described [27]. Briefly, liver tissues were digested with 0.05% collagenase IV (Sigma-Aldrich, Germany) and 0.1 mg/ml DNase I (Merck,

Germany), followed by density-gradient centrifugation using 30% Percoll (Cytiva, United Kingdom).

Myeloperoxidase activity assay

Myeloperoxidase (MPO) activity in tissue homogenates was measured using a commercial MPO activity assay kit (Solarbio, Beijing, China) according to the manufacturer's instructions.

Enzyme-linked immunosorbent assay

Neutrophil elastase levels in tissue samples were quantified using a commercial enzyme-linked immunosorbent assay kit (MLbio, China) according to the manufacturer's instructions.

Statistics

Data are presented as mean ± standard error of the mean (SEM). Survival was analyzed using the log-rank test. Longitudinal bioluminescence data were analyzed by two-way analysis of variance (ANOVA) with multiple comparisons. Comparisons among 3 groups were performed using one-way ANOVA with multiple-comparison testing, whereas comparisons between 2 groups were performed using an unpaired 2-tailed Student t test. The Mann-Whitney U test was used for data that did not meet assumptions of normality. Statistical analyses were performed using Prism version 10 (GraphPad Software). $P < .05$ was considered statistically significant. P values are denoted as follows: *$P < 0.05$; **$P < .01$; ***$P < 0.001$; ****$P < 0.0001$.

Results

aGVHD is associated with vascular injury and functional impairment of bone marrow-derived EPCs

We established a major MHC-mismatched aGVHD model by transplanting C57BL/6 bone marrow cells and splenocytes into lethally irradiated BALB/c recipients, with syngeneic transplantation serving as the non-GVHD control. Allogeneic recipients developed progressive clinical aGVHD with weight loss, increased clinical scores, and reduced survival compared with syngeneic controls (Fig. 1A-C). Histopathologic examination confirmed aGVHD target organs injury, characterized by inflammatory cells infiltration and hepatocellular damage in the liver and epithelial injury with crypt destruction in the small intestine and colon (Fig. 1D), pathology scores were increased in the liver, small intestine, and colon of aGVHD recipients compared with syngeneic controls (Fig. 1E).

To characterize vascular injury during aGVHD, we examined endothelium of C57BL/6-to-BALB/c transplant recipients and syngeneic controls. At day 15 after HSCT, transmission electron microscopy (TEM) revealed disrupted endothelial junctional structures and increased plasma membrane vesicles in the colon, together with endothelial swelling and altered sinusoidal fenestral architecture in the liver of aGVHD recipients (Fig. 2A). Consistent with these changes, immunofluorescence analysis showed significantly reduced α-SMA coverage of $CD31^+$ vessels in both the colon and liver of aGVHD recipients, indicating loss of perivascular support [15] (Fig. 2B). ZO-1 expression on $CD31^+$ endothelial cells were also markedly reduced, further demonstrating impaired endothelial junctional integrity (Fig. 2C). To assess vascular architecture, we performed light-sheet fluorescence microscopy after in vivo labeling with an anti-CD31 antibody. Three-dimensional reconstructions revealed tissue-specific alterations in $CD31^+$ vascular structures, with changes in bone marrow vascular mesh organization and a more prominent vascular meshwork in the liver and colon (Fig. 2D-F, supplementary video 1-3). In the analyzed reconstructions, vascular volume density, vascular length density, and branch density were higher in the colon and modestly higher in the liver of aGVHD recipients, whereas all three

measures were modestly lower in the bone marrow (Fig. 2G). Higher-magnification images further illustrated alterations in local vascular organization (Fig. 2H). Evans blue extravasation was increased in the liver and colon, demonstrating impaired vascular barrier function (Fig. 2I). These findings suggest tissue-specific vascular remodeling during aGVHD.

We next identified bone marrow EPCs based on their Sca-1, CD34 and CD309 expression [28,29]. EPC frequency was increased in aGVHD recipients at day 15 after HSCT (Fig. 3A). Despite this increase, EPCs exhibited reduced CCK-8 activity and increased apoptosis compared with those from syngeneic controls (Fig. 3B and C). By day 21, bone marrow EPC frequency was lower in aGVHD recipients (Fig. 3D). EPCs from aGVHD recipients also displayed impaired adhesion and migration and increased intracellular ROS levels (Fig. 3E-G). Together, these findings suggest that aGVHD is associated with time-dependent vascular injury and impaired EPC function.

Neutrophil-mediated EPC injury during aGVHD is associated with RIPK1–MLKL signaling

We next examined neutrophil infiltration and activation during aGVHD. On day 15 after HSCT, aGVHD recipients exhibited increased absolute numbers of $CD11b^{+}Ly6G^{+}$ neutrophils in the colon and liver compared with syngeneic controls. Neutrophil frequency was increased in the liver but unchanged in the colon (Fig. 4A). In the spleen, neutrophil frequency was reduced, whereas absolute numbers were not significantly different between groups (Fig. 4A). Intracellular ROS levels were increased in liver and colon infiltrated neutrophils but not in splenic neutrophils (Fig. 4B). In addition, liver and colon infiltrated neutrophils also showed increased frequencies of pro-IL-$1\beta^{+}$ and TNF-α^{+} cells (Fig. 4C-D). Bone marrow neutrophils from aGVHD recipients exhibited increased $CitH3^{+}$ area per $Ly6G^{+}$ cell, indicating enhanced NETs formation (Fig. 4E).

To determine whether neutrophils from aGVHD recipients could induce EPC injury, we cocultured them with bone marrow-derived EPCs from wild-type C57BL/6 mice at an EPC-to-neutrophil ratio of 1:20 for 6 hours. Coculture increased the percentage of Annexin V^+ EPCs (Fig. 4F) and reduced CCK-8 absorbance compared with EPC monoculture, while addition of DNase I significantly increased CCK-8 absorbance relative to untreated cocultures (Fig. 4G). These findings suggest NETs-associated DNA contributes to neutrophil-induced EPC injury. Having identified a NETs associated neutrophil-induced EPC injury, we next explore the cell-death pathways associated with EPC dysfunction. We focused on RIPK1-MLKL signaling because of its involvement in inflammatory cell death [30-33]. Immunoblot analysis revealed increased RIPK1 and phosphorylated MLKL (p-MLKL) protein levels in EPCs from the bone marrow of aGVHD recipients compared with syngeneic controls (Fig. 4H). Together, these findings suggest that NET-associated extracellular DNA contributes to neutrophil-induced EPC injury and that EPC apoptosis in aGVHD is associated with activation of RIPK1–MLKL signaling.

Pharmacologic RIPK1 inhibition improves EPC function and attenuates aGVHD

Given the increased RIPK1 and p-MLKL levels in EPCs during aGVHD, we next tested whether pharmacologic RIPK1 inhibition could improve EPC function and ameliorate aGVHD. Beginning on day 7 after HSCT, aGVHD recipients received the RIPK1 inhibitor ORIC-559 (40 mg/kg, twice daily) or vehicle by oral gavage. ORIC-559 improved survival, attenuated body weight loss, and reduced clinical aGVHD scores compared with vehicle treatment (Fig. 5A-C). Histopathologic analysis on day 20 showed reduced hepatic inflammatory infiltration and intestinal mucosal injury, accompanied by lower pathology scores in the liver, small intestine, and colon (Fig. 5D).

ORIC-559 also reduced Evans blue extravasation in the colon and liver, indicating improved vascular barrier function (Fig. 5E). EPCs isolated from ORIC-559-treated recipients on day 20 exhibited a lower frequency of Annexin V^+ cells and higher CCK-8 absorbance than those from vehicle-treated recipients (Fig. 5F-G). EPC adhesion and transwell migration were also improved (Fig. 5H-I), suggesting a beneficial effect of RIPK1 inhibition on EPC survival and function. Since the activated neutrophils mediated EPC injury, we next assessed neutrophil oxidative activity and tissue infiltration following RIPK1 inhibition. ORIC-559 reduced intracellular ROS levels in $CD11b^+Ly6G^+$ neutrophils from the colon, liver, and spleen (Fig. 5J). Absolute neutrophil numbers were reduced in the colon and liver but increased in the spleen (Fig. 5K), indicating tissue-specific changes in neutrophil abundance. Together, these findings suggest that pharmacologic RIPK1 inhibition improved EPC survival and function, reduced vascular leakage and neutrophil oxidative activity, and amelioration of aGVHD.

Ex vivo-expanded EPCs suppress neutrophil oxidative activity and NETs formation

Since EPC has been reported to regulate T cells function in the GVHD [18], we next asked whether EPCs could, in turn, restrain neutrophil activation. Bone marrow-derived EPCs from wild-type C57BL/6 mice were expanded ex vivo and characterized before coculture. These cells expressed Sca-1, CD34, CD309, and CD31, with minimal CD45 staining compared to the isotype control (Fig. 6A). They exhibited endothelial-like morphology at the first passage and formed capillary-like networks on Matrigel (Fig. 6B-D). Bone marrow neutrophils from aGVHD recipients were cultured alone or with EPCs at an EPC-to-neutrophil ratio of 1:1 for 4 hours, either in direct contact or separated by a transwell membrane. Intracellular ROS levels in $CD11b^+Ly6G^+$ neutrophils were significantly lower in both coculture conditions than in neutrophil monoculture. No significant difference was detected between direct and transwell coculture (Fig. 6E), indicating that direct cell-cell contact was not required for EPC-mediated

suppression of neutrophil ROS accumulation. Direct coculture with EPCs also reduced $CitH3^+$ area per $Ly6G^+$ cell, consistent with decreased NETs formation (Fig. 6F). The percentage of live neutrophils did not differ significantly among monoculture, direct coculture, and transwell coculture (Fig. 6G). Together, these findings suggest that EPCs suppress neutrophil oxidative activity without requiring direct cell–cell contact and reduce NETs formation without a detectable decrease in neutrophil viability.

EPC administration attenuates aGVHD and reduces vascular injury

Since in vitro-expanded EPCs were capable of suppressing neutrophil activation, we next evaluated their effects in vivo. aGVHD recipients received EPCs (1×10^6 cells per mouse per injection) or vehicle according to the diagram shown in Fig. 7A, with EPC transfusion on days 0, 9, 14, and 21 after HSCT. EPC treatment improved survival compared with vehicle treatment (Fig. 7B). The proportion of mice without diarrhea was also higher in the EPC-treated group on days 25-30 post-HSCT (Fig. 7C). Histopathologic analysis on day 15 showed reduced inflammatory cells infiltration and tissue injury, indicating by lower pathology scores in the liver, small intestine, and colon (Fig. 7D). EPC transfusion reduced Evans blue extravasation in the liver and colon, indicating improved vascular barrier function (Fig. 7E). A lower density of $TUNEL^+CD31^+$ cells in the colon of recipients with EPC treatment compared to the vehicle group, suggesting a reduction of endothelial apoptosis (Fig. 7F). Flow cytometry analysis further revealed reduced frequencies of Annexin V^+, ROS^+, and MHC class II^+ endothelial cells in the liver (Fig. 7G-I), indicating EPC transfusion attenuated endothelial injury and oxidative stress in multiple aGVHD target organs. We next examined whether EPC transfusion also impacts on neutrophil activation and inflammatory function. Indeed, EPC-treated recipients exhibited lower frequencies of $CD11b^+Ly6G^+$ neutrophils in the liver and colon (Fig. 7J-K). MPO activity and neutrophil elastase (NE) concentrations were also reduced in both tissues (Fig. 7L-M). Together,

these findings demonstrate that EPC administration attenuates aGVHD in association with reduced vascular leakage, endothelial injury, and neutrophil-mediated inflammation.

EPC administration preserves graft-versus-leukemia (GVL) activity

Having shown that EPC administration attenuates aGVHD, we next examined whether it compromises GVL activity. Lethally irradiated BALB/c recipients received luciferase-expressing A20 lymphoma cells together with T cell-depleted bone marrow (TCD-BM), with or without donor splenocytes from C57BL/6 donors. Progressive tumor expansion in recipients receiving TCD-BM without donor splenocytes, while recipients receiving donor splenocytes from both vehicle- and EPC-treated group showed substantially lower bioluminescent signals than the TCD-BM group (Fig. 8A-C). EPC administration improved survival, with 80% of EPC-treated recipients alive on day 30, compared with no surviving vehicle-treated recipients (Fig. 8A-C). Low tumor-associated bioluminescence was maintained through day 30 in EPC-treated recipients, indicating preservation of GVL activity during EPC treatment.

To assess whether EPC administration impact on $CD8^+$ T-cell cytotoxicity function in the lymphoid organ, we quantified $CD8^+$ T cells and their cytokine expression in the spleen on day 15 after HSCT. No significant differences in the frequency or absolute number of $CD8^+$ T cells were detected between EPC- and vehicle-treated recipients (Fig. 8D-E), or in the proportions of IFN-γ^+ and TNF-α^+ cells among $CD8^+$ T cells (Fig. 8F-G). Together, these findings suggest that EPC administration preserves GVL activity in association with maintaining functional $CD8^+$ T cells.

Discussion

Severe aGVHD remains a lethal complication after allo-HSCT, endothelial damage and impaired vascular repair are associated with severe aGVHD [15,17,18,34]. Treatment of aGVHD largely

relies on systemic immunosuppression, which can increase the risk of infection and may not achieve a complete response in some patients [35-39]. A randomized phase 3 trial showed that adding mesenchymal stromal cells to basiliximab and calcineurin inhibitor therapy improved response rates in patients with steroid-resistant aGVHD [40]. Our study identifies a reciprocal interaction between neutrophils and EPCs that connects innate inflammatory activity with the vascular repair. Neutrophils from aGVHD recipients induced EPC injury in association with RIPK1 signaling, while EPCs suppressed neutrophil oxidative activity and NETs formation. EPC transfusion and pharmacologic RIPK1 inhibition each improved vascular integrity and ameliorated aGVHD, more important, EPC transfusion maintains GVL effect. These findings highlight the therapeutic potential of EPC transfusion in the setting of aGVHD.

EPCs support vascular homeostasis through regenerative and paracrine actions [16]. Clinical studies have linked EPC impairment or altered EPC recovery to aGVHD [17,34], and EPC administration can ameliorate experimental GVHD-associated endothelial injury [18]. Our findings provide a functional perspective on these observations. Increased EPC frequency early after HSCT coexisted with oxidative stress, apoptosis, and impaired adhesion and migration, followed by the reduction of EPC later after HSCT. This pattern suggests that the early increase in the EPC compartment is insufficient to sustain effective repair during ongoing inflammation. Three-dimensional image further revealed tissue-specific vascular remodeling, with higher density measures in the colon and liver and modestly lower values in the bone marrow. The increased vascular leakage suggests that vascular structure, barrier function, and repair capacity play an important role in the pathogenesis of aGVHD. This perspective integrates the vascular compartment into the broader concept of aGVHD as a disorder of tissue injury and regeneration [8].

A key finding is that activated neutrophils can impair endogenous vascular repair. Donor-derived neutrophils from aGVHD recipients enhanced NETs formation and increased EPC apoptosis, reduced CCK-8 activity. Disruption of NETs with DNase I attenuated EPC injury by neutrophils, suggests a NETs-associated mechanism to EPC injury. These observations connect neutrophil activation with functional deterioration of the vascular repair compartment, provide a potential explanation for persistent endothelial vulnerability in the setting of aGVHD. They also identify extracellular DNA-containing structures as a candidate target for preserving EPC function within an inflammatory environment.

The activation of RIPK1 signaling in EPC findings provide a pharmacologic link between inflammatory cell-death signaling and vascular protection. RIPK1 coordinates inflammatory and cell-death pathways, while MLKL functions as an effector of necroptotic cell death [30-33]. Prado-Acosta et al. demonstrated that RIP1 inhibition protected intestinal stem cells from apoptosis and reduced GVHD mortality [41], and Yu et al. identified an MLKL-independent RIPK1/RIPK3 inflammatory pathway in intestinal epithelial cells [42]. Our study extends this therapeutic framework to the vascular repair compartment. EPCs from aGVHD recipients exhibited increased RIPK1 and p-MLKL levels, while ORIC-559 treatment improved EPC survival, adhesion, migration and reduced vascular leakage. ORIC-559 treatment also reduced neutrophil infiltration and ROS production in the GVHD target organs colon and liver, highlight the potential of RIPK1 inhibition to preserve EPC function and vascular integrity while attenuating neutrophil-associated inflammation in aGVHD.

The ability of EPCs to restrain neutrophil responses broadens their therapeutic relevance beyond vascular regeneration. EPCs can regulate inflammation through paracrine mechanisms [16], and studies of EPCs, mesenchymal stromal cells, and mature endothelial cells have described

immunoregulatory effects on macrophages or T cells [43-46]. Arsenic trioxide-loaded extracellular vesicles from human umbilical cord-derived mesenchymal stromal cells also reduced aGVHD severity by modulating macrophage polarization in mice [47]. Here, we showed EPCs reduced neutrophil ROS in both direct and transwell coculture, supporting a mechanism that does not require direct cell-cell contact. Direct coculture also reduced NETs formation without a detectable decline in neutrophil viability, suggesting that EPCs can help constrain neutrophils inflammatory activity while supporting vascular homeostasis. Persistence of ROS suppression across a Transwell membrane also provides a rationale for exploring EPC-derived mediators as potential therapeutic candidates.

The reciprocal effects seen in vitro may help explain why EPC administration reduced vascular injury and inflammation in vivo. Activated neutrophils can compromise EPC function, while functional EPCs can restrain neutrophil activation. Preserving or replenishing this regulatory capacity may help interrupt inflammatory amplification within injured tissues. Consistent with this model, EPC administration reduced vascular leakage, endothelial apoptosis, and the frequencies of ROS^+ and MHC class II^+ endothelial cells. The neutrophil frequencies, MPO activity, and NE concentrations were also reduced in the aGVHD target organs. These coordinated changes support a dual therapeutic role for EPCs in vascular protection and regulation of neutrophil-associated inflammation, linking preservation of the vascular barrier with improved tissue homeostasis.

EPC administration reduced vascular injury and inflammation while preserving GVL activity. In the A20 lymphoma cells challenge model, recipients with EPC-treated showed clearance of tumor burden and achieved 80% survival on day 30. More importantly, the donor $CD8^+$ T-cell number and function from the EPC treated recipients did not differ significantly from vehicle controls.

Together, these findings support EPC transfusion improved survival with preserved GVL activity. Previous RIPK1 studies have similarly shown GVHD attenuation with maintenance of GVL activity [41,42,48]. A retrospective study of patients with active acute myeloid leukemia undergoing haploidentical transplantation with post-transplant cyclophosphamide found no association between GVHD and a lower relapse incidence [49]. This convergence highlights protection of target-tissue homeostasis as a promising approach to limiting GVHD while retaining the GVL effect of transplantation.

Several limitations warrant further investigation. Cell type-specific perturbation of RIPK1, RIPK3, and MLKL, together with NETs-targeted approaches will help define how extracellular DNA and cell-death signaling contribute to EPC dysfunction. Characterizing the mediators and in vivo fate of EPCs will clarify their vascular and immunoregulatory actions. Current EPC transfusion regimen included administration on day 0, a delayed-treatment protocol is needed to assess efficacy against established aGVHD. Additional transplant and leukemia models, long-term follow-up, and human-derived cell validation will further define durability and translational applicability.

Conclusions

This study identifies reciprocal neutrophil–EPC interactions that link innate inflammation to impaired vascular repair in aGVHD. RIPK1 inhibition protects EPC function and vascular integrity, while EPC administration reduces vascular injury and neutrophil-associated inflammation and ameliorates aGVHD while preserving GVL activity.

List of abbreviations

aGVHD	Acute graft-versus-host disease
allo-HSCT	Allogeneic hematopoietic stem cell transplantation
ANOVA	Analysis of variance
APCs	Antigen-presenting cells
CCK-8	Cell Counting Kit-8
CD	Cluster of differentiation
CitH3	Citrullinated histone H3
DAPI	4′,6-Diamidino-2-phenylindole
DCFH-DA	2′,7′-Dichlorodihydrofluorescein diacetate
DNase I	Deoxyribonuclease I
EASIX	Endothelial activation and stress index
ECs	Endothelial cells
ELISA	Enzyme-linked immunosorbent assay
EPCs	Endothelial progenitor cells
FBS	Fetal bovine serum
GAPDH	Glyceraldehyde-3-phosphate dehydrogenase
GFP	Green fluorescent protein
GI	Gastrointestinal
GVHD	Graft-versus-host disease
GVL	Graft-versus-leukemia
H&E	Hematoxylin and eosin

HSCT	Hematopoietic stem cell transplantation
IFN-γ	Interferon gamma
IL-1β	Interleukin-1 beta
IRF1	Interferon regulatory factor 1
mAbs	Monoclonal antibodies
MFI	Mean fluorescence intensity
MHC	Major histocompatibility complex
MLKL	Mixed lineage kinase domain-like protein
MPO	Myeloperoxidase
NE	Neutrophil elastase
NETs	Neutrophil extracellular traps
PBS	Phosphate-buffered saline
PD-L1	Programmed death-ligand 1
PFA	Paraformaldehyde
p-MLKL	Phosphorylated mixed lineage kinase domain-like protein
RIPA	Radioimmunoprecipitation assay
RIPK1	Receptor-interacting serine/threonine-protein kinase 1
RIPK3	Receptor-interacting serine/threonine-protein kinase 3
ROS	Reactive oxygen species
Sca-1	Stem cell antigen-1
SDS	Sodium dodecyl sulfate

SEM	Standard error of the mean
TCD-BM	T cell-depleted bone marrow
TCR	T-cell receptor
TEM	Transmission electron microscopy
TNF-α	Tumor necrosis factor alpha
Tregs	Regulatory T cells
TUNEL	Terminal deoxynucleotidyl transferase-mediated dUTP nick-end labeling
VEGF	Vascular endothelial growth factor
VLD	Vascular length density
VVD	Vascular volume density
ZO-1	Zonula occludens-1
α-SMA	Alpha-smooth muscle actin

Declarations

Ethics approval and consent to participate: All animal procedures were approved by the Institutional Animal Care and Use Committee of Army Medical University (approval no. AMUWEC20245225) and performed in accordance with the approved protocols. Consent to participate was not applicable because this study did not involve human participants.

Consent for publication: Not applicable.

Availability of data and materials: All data supporting the findings of this study are included in this article and its supplementary information files.

Competing interests: The authors declare that they have no competing interests.

Funding: This work was supported by the National Key Research and Development Program of China 2022YFA1103304 (to X.Z.)，Chemical Poisoning Key Research Project 2024K004 (to X.Z.)，the Special Project for Talent Construction in Xinqiao Hospital 2022XKRC001 (to X.Z.), National Natural Science Foundation of China 82670310 (to Q.S.) , National Natural Science Foundation of China 82600479 (to X.X.), Natural Science Foundation of Chongqing CSTB2023NSCQ-MSX0260 (to R.W.).

Authorship Contributions: Y.K., X.X., R.W., and F.T. performed the experiments and conducted the formal data analysis. Q.S. and X.Z. performed the investigation and interpreted the data, Y.K. and Q.S. wrote the manuscript, Q.S. and X.Z. reviewed and edited the manuscript, Q.S. and X.Z. administered, coordinated the project and acquired funding for the study.

Acknowledgments: The authors thank the animal facility, flow cytometry core, and pathology core in Xinqiao Hospital and Jinfeng Laboratory.

Reference

1. Zeiser R, Blazar BR. Acute graft-versus-host disease - biologic process, prevention, and therapy. N Engl J Med. 2017; 377:2167-79.

2. Chen Y, Xu Y, Wu D. Advances in graft-versus-host disease prevention strategies: latest updates from the 2022 ASH annual meeting. Exp Hematol Oncol. 2023; 12:59.

3. Fu YY, Egorova A, Sobieski C, Kuttiyara J, Calafiore M, Takashima S, et al. T cell recruitment to the intestinal stem cell compartment drives immune-mediated intestinal damage after allogeneic transplantation. Immunity. 2019; 51:90-103.e3.

4. Dietrich S, Falk CS, Benner A, Karamustafa S, Hahn E, Andrulis M, et al. Endothelial vulnerability and endothelial damage are associated with risk of graft-versus-host disease and response to steroid treatment. Biol Blood Marrow Transplant. 2013; 19:22-7.

5. Yazdanparast S, Abroun S, Rostami T, Mohammadi S. Clinical and translational advances in regulatory T cell-based strategies in allogeneic hematopoietic stem cell transplantation: highlights from ASH 2025. Exp Hematol Oncol. 2026; 15:40.

6. Biedermann BC. Vascular endothelium and graft-versus-host disease. Best Pract Res Clin Haematol. 2008; 21:129-38.

7. Neidemire-Colley L, Robert J, Ackaoui A, Dorrance AM, Guimond M, Ranganathan P. Role of endothelial cells in graft-versus-host disease. Front Immunol. 2022; 13:1033490.

8. Chakraverty R, Teshima T. Graft-versus-host disease: a disorder of tissue regeneration and repair. Blood. 2021; 138:1657-65.

9. Salat C, Holler E, Kolb HJ, Pihusch R, Reinhardt B, Hiller E. Endothelial cell markers in bone marrow transplant recipients with and without acute graft-versus-host disease. Bone Marrow Transplant. 1997; 19:909-14.

10. Tichelli A, Gratwohl A. Vascular endothelium as 'novel' target of graft-versus-host disease. Best Pract Res Clin Haematol. 2008; 21:139-48.

11. Pedraza A, Salas MQ, Rodríguez-Lobato LG, Escribano-Serrat S, Suárez-Lledo M, Martínez-Cebrian N, et al. EASIX score correlates with endothelial dysfunction biomarkers and predicts

603 risk of acute graft-versus-host disease after allogeneic transplantation. Transplant Cell Ther. 2024;
604 30:187. e1-187.e12.
605 12. Gafken PR, Paczesny S. Blood proteomics for quantitative biomarkers of cellular therapies.
606 Biomark Res. 2025;13:120.
607 13. Hahn T, Zhao Q, Miller EG, Elder P, Langenberg L, Luebbering N, et al. TA-TMA and
608 GVHD are distinct consequences of endothelial injury: a MIDAS consortium study. Blood Adv.
609 2026; 10:5076-86.
610 14. Neidemire-Colley L, Kumar R, Garfinkle EA, Steere C, Gordon A, Giordano G, et al.
611 Recipient endothelial IRF1 mediates IFNγ-driven tissue tolerance in mouse models of acute graft-
612 versus-host disease. Blood. 2026; doi:10.1182/blood.2026033806.
613 15. Cordes S, Mokhtari Z, Bartosova M, Mertlitz S, Riesner K, Shi Y, et al. Endothelial damage
614 and dysfunction in acute graft-versus-host disease. Haematologica. 2021; 106:2147-60.
615 16. Hassanpour M, Salybkov AA, Kobayashi S, Asahara T. Anti-inflammatory prowess of
616 endothelial progenitor cells in the realm of biology and medicine. NPJ Regen Med. 2024; 9:27.
617 17. Cao XN, Kong Y, Song Y, Shi MM, Zhao HY, Wen Q, et al. Impairment of bone marrow
618 endothelial progenitor cells in acute graft-versus-host disease patients after allotransplant. Br J
619 Haematol. 2018; 182:870-86.
620 18. Wang W, Ye Y, Du Y, Xu Z, Yuan K, Wang Y, et al. EPC infusion ameliorates acute graft-
621 versus-host disease-related endothelial injury after allogeneic bone marrow transplantation. Front
622 Immunol. 2022; 13:1019657.
623 19. Hülsdünker J, Ottmüller KJ, Neeff HP, Koyama M, Gao Z, Thomas OS, et al. Neutrophils
624 provide cellular communication between ileum and mesenteric lymph nodes at graft-versus-host
625 disease onset. Blood. 2018; 131:1858-69.

626 20. Schwab L, Goroncy L, Palaniyandi S, Gautam S, Triantafyllopoulou A, Mocsai A, et al.
627 Neutrophil granulocytes recruited upon translocation of intestinal bacteria enhance graft-versus-
628 host disease via tissue damage. Nat Med. 2014; 20:648-54.
629 21. An S, Raju I, Surenkhuu B, Kwon JE, Gulati S, Karaman M, et al. Neutrophil extracellular
630 traps (NETs) contribute to pathological changes of ocular graft-vs.-host disease (oGVHD) dry
631 eye: implications for novel biomarkers and therapeutic strategies. Ocul Surf. 2019; 17:589-614.
632 22. Tugues S, Amorim A, Spath S, Martin-Blondel G, Schreiner B, De Feo D, et al. Graft-versus-
633 host disease, but not graft-versus-leukemia immunity, is mediated by GM-CSF-licensed myeloid
634 cells. Sci Transl Med. 2018;10: eaat8410.
635 23. Dai H, Zhang C, Zhang H, Jiang C, Huang X, Dai S, et al. Donor-derived distinct neutrophil
636 subsets in the G-CSF-mobilized peripheral blood grafts predict acute GVHD development.
637 Transplant Cell Ther. 2026; doi: 10.1016/j.jtct.2026.08.042.
638 24. Ni X, Song Q, Cassady K, Deng R, Jin H, Zhang M, et al. PD-L1 interacts with CD80 to
639 regulate graft-versus-leukemia activity of donor CD8+ T cells. J Clin Invest. 2017; 127:1960-77.
640 25. Kaplan DH, Anderson BE, McNiff JM, Jain D, Shlomchik MJ, Shlomchik WD. Target
641 antigens determine graft-versus-host disease phenotype. J Immunol. 2004; 173:5467-75.
642 26. Radu M, Chernoff J. An in vivo assay to test blood vessel permeability. J Vis Exp. 2013;(73):
643 e50062.
644 27. Sokol L, Geldhof V, García-Caballero M, Conchinha NV, Dumas SJ, Meta E, et al. Protocols
645 for endothelial cell isolation from mouse tissues: small intestine, colon, heart, and liver. STAR
646 Protoc. 2021; 2:100489.
647 28. Lin YW, Huang CY, Chen YH, Shih CM, Tsao NW, Lin CY, et al. GroEL1, a heat shock
648 protein 60 of Chlamydia pneumoniae, impairs neovascularization by decreasing endothelial
649 progenitor cell function. PLoS One. 2013;8: e84731.

650 29. Marrotte EJ, Chen DD, Hakim JS, Chen AF. Manganese superoxide dismutase expression in
651 endothelial progenitor cells accelerates wound healing in diabetic mice. J Clin Invest. 2010;
652 120:4207-19.
653 30. Sun L, Wang H, Wang Z, He S, Chen S, Liao D, et al. Mixed lineage kinase domain-like
654 protein mediates necrosis signaling downstream of RIP3 kinase. Cell. 2012; 148:213-27.
655 31. Weinlich R, Oberst A, Beere HM, Green DR. Necroptosis in development, inflammation and
656 disease. Nat Rev Mol Cell Biol. 2017; 18:127-36.
657 32. Clucas J, Meier P. Roles of RIPK1 as a stress sentinel coordinating cell survival and
658 immunogenic cell death. Nat Rev Mol Cell Biol. 2023; 24:835-52.
659 33. Yuan J, Ofengeim D. A guide to cell death pathways. Nat Rev Mol Cell Biol. 2024; 25:379-
660 95.
661 34. Takamatsu A, Nakashima Y, Haji S, Tsuda M, Masuda T, Kimura D, et al. Circulating
662 endothelial cells and endothelial progenitor cells as potential predictors of acute GVHD after
663 allogeneic hematopoietic stem cell transplantation. Eur J Haematol. 2022; 109:146-53.
664 35. Malard F, Huang XJ, Sim JPY. Treatment and unmet needs in steroid-refractory acute graft-
665 versus-host disease. Leukemia. 2020; 34:1229-40.
666 36. Martin PJ. How I treat steroid-refractory acute graft-versus-host disease. Blood. 2020;
667 135:1630-8.
668 37. Reed FE, DeFilipp Z. Innovative approaches in acute graft-versus-host disease: emerging
669 therapeutics and novel clinical trial design. Leuk Lymphoma. 2026; 67:803-12.
670 38. Robles JD, Liu YP, Cao J, Xiang Z, Cai Y, Manio M, et al. Immunosuppressive mechanisms
671 of human bone marrow derived mesenchymal stromal cells in BALB/c host graft versus host
672 disease murine models. Exp Hematol Oncol. 2015; 4:13.

673 39. Liu Y, Zhao Y, Qi J, Ma X, Qi X, Wu D, et al. Fecal microbiota transplantation combined
674 with ruxolitinib as a salvage treatment for intestinal steroid-refractory acute GVHD. Exp Hematol
675 Oncol. 2022; 11:96.
676 40. Zhao K, Lin R, Fan Z, Chen X, Wang Y, Huang F, et al. Mesenchymal stromal cells plus
677 basiliximab, calcineurin inhibitor as treatment of steroid-resistant acute graft-versus-host disease:
678 a multicenter, randomized, phase 3, open-label trial. J Hematol Oncol. 2022;15:22.
679 41. Prado-Acosta M, Jeong S, Utrero-Rico A, Goncharov T, Webster JD, Holler E, et al.
680 Inhibition of RIP1 improves immune reconstitution and reduces GVHD mortality while
681 preserving graft-versus-leukemia effects. Sci Transl Med. 2023 ;15: eadf8366.
682 42. Yu X, Ma H, Li B, Ji Y, Du Y, Liu S, et al. A novel RIPK1 inhibitor reduces GVHD in mice
683 via a nonimmunosuppressive mechanism that restores intestinal homeostasis. Blood.
684 2023 ;141 :1070-86.
685 43. Zullo JA, Nadel EP, Rabadi MM, Baskind MJ, Rajdev MA, Demaree CM, et al. The
686 secretome of hydrogel-coembedded endothelial progenitor cells and mesenchymal stem cells
687 instructs macrophage polarization in endotoxemia. Stem Cells Transl Med. 2015 ;4 :852-61.
688 44. Song WJ, Li Q, Ryu MO, Ahn JO, Ha Bhang D, Chan Jung Y, et al. TSG-6 secreted by
689 human adipose tissue-derived mesenchymal stem cells ameliorates DSS-induced colitis by
690 inducing M2 macrophage polarization in mice. Sci Rep. 2017; 7:5187.
691 45. Lim WC, Olding M, Healy E, Millar TM. Human endothelial cells modulate CD4+ T cell
692 populations and enhance regulatory T cell suppressive capacity. Front Immunol. 2018; 9:565.
693 46. Taflin C, Favier B, Baudhuin J, Savenay A, Hemon P, Bensussan A, et al. Human endothelial
694 cells generate Th17 and regulatory T cells under inflammatory conditions. Proc Natl Acad Sci U
695 S A. 2011; 108:2891-6.

47. Su Y, Sun X, Liu X, Qu Q, Yang L, Chen Q, et al. hUC-EVs-ATO reduce the severity of acute GVHD by resetting inflammatory macrophages toward the M2 phenotype. J Hematol Oncol. 2022;15:99.

48. Hill GR, Koyama M. A novel RIPK1 inhibitor attenuates GVHD. Blood. 2023; 141:969-70.

49. Baron F, Labopin M, Tischer J, Raiola AM, Vydra J, Blaise D, et al. GVHD occurrence does not reduce AML relapse following PTCy-based haploidentical transplantation: a study from the ALWP of the EBMT. J Hematol Oncol. 2023;16:10.

Figures and figure legends

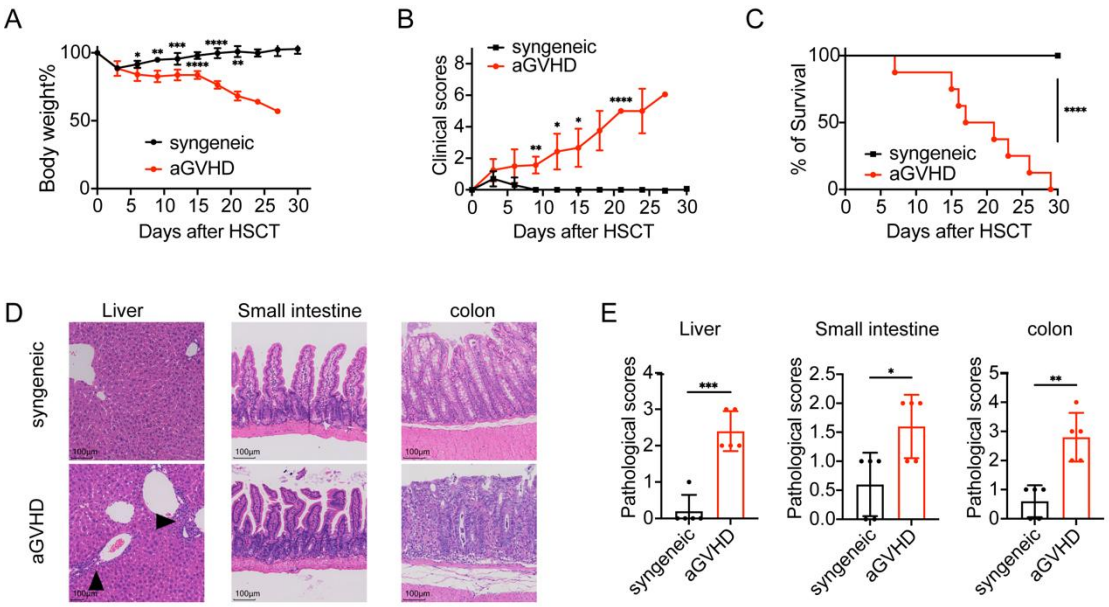

Figure 1. Establishment of murine aGVHD and characterization of tissue injury and vascular remodeling. Lethally irradiated (7.5 Gy) BALB/c recipients were transplanted with bone marrow cells (5×10^6) and splenocytes (1.25×10^6) from C57BL/6 donors. Syngeneic BALB/c-to-BALB/c transplantation served as the non-GVHD control. **(A-C)** Body weight, expressed as a percentage of baseline (A), clinical aGVHD scores (B), and survival (C) after HSCT (n = 8-10 per group). **(D-E)** Representative H&E-stained sections of the liver, small intestine, and colon on day 15 after HSCT (D), with corresponding histopathologic scores (E; n = 5 per group). Arrowheads indicate inflammatory cell infiltrates in the liver. Scale bars, 100 μm. Data in A, B, and E are presented as mean ± SEM; results are from two experiments. Statistical significance was assessed using two-way ANOVA (A-B), the log-rank test (C), or unpaired two-tailed Student t tests (E). *$P < 0.05$; **$P < 0.01$; ***$P < 0.001$; ****$P < 0.0001$.

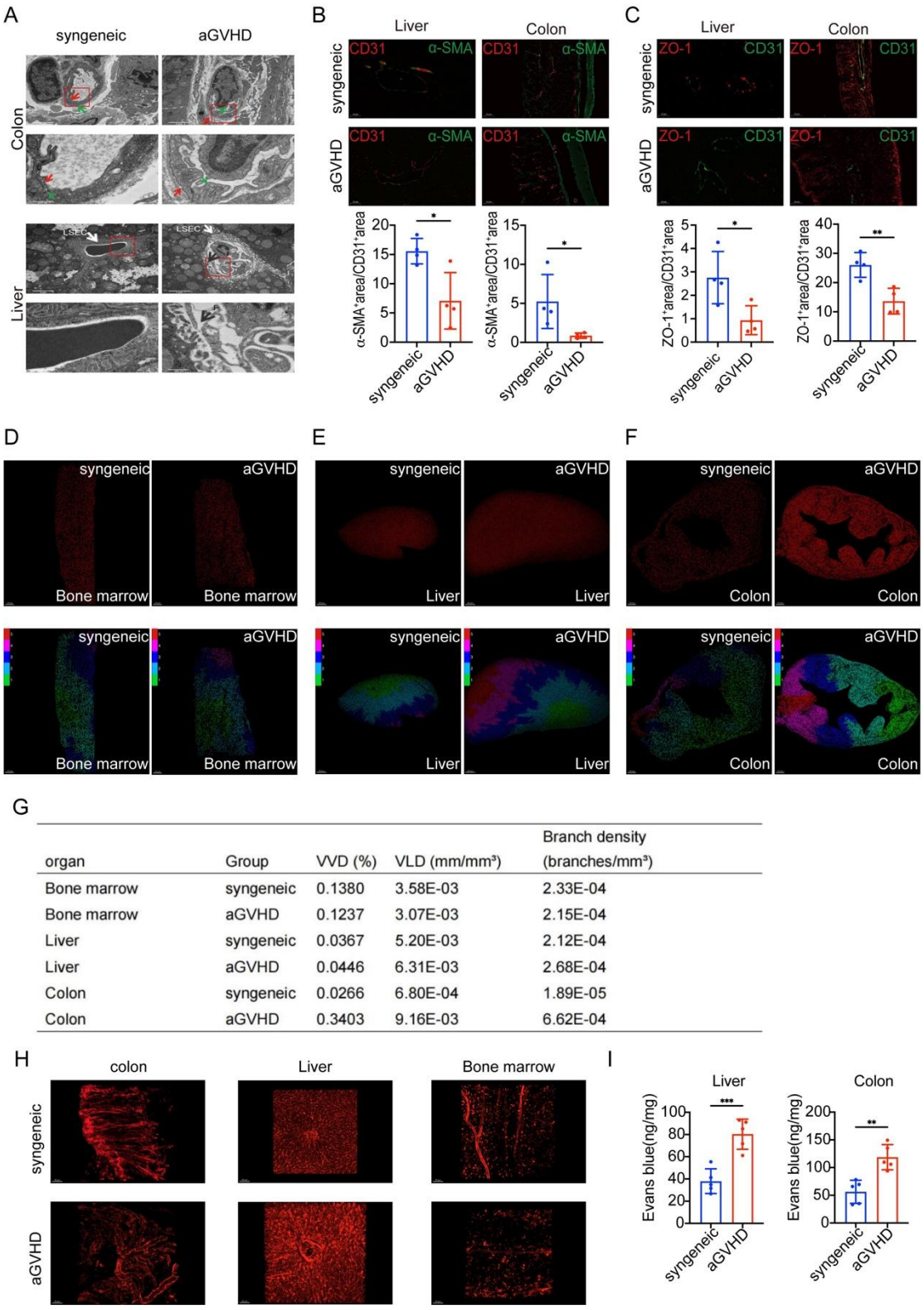

G

organ	Group	VVD (%)	VLD (mm/mm³)	Branch density (branches/mm³)
Bone marrow	syngeneic	0.1380	3.58E-03	2.33E-04
Bone marrow	aGVHD	0.1237	3.07E-03	2.15E-04
Liver	syngeneic	0.0367	5.20E-03	2.12E-04
Liver	aGVHD	0.0446	6.31E-03	2.68E-04
Colon	syngeneic	0.0266	6.80E-04	1.89E-05
Colon	aGVHD	0.3403	9.16E-03	6.62E-04

Figure 2. aGVHD is associated with vascular injury. aGVHD was established as described in Figure 1. Syngeneic transplantation served as control. Tissues were collected on day 15 unless

otherwise indicated. **(A)** Representative transmission electron microscopy images of endothelial ultrastructure in the colon and liver. Red arrows indicate endothelial tight-junction regions; green arrows, endothelial plasma membrane vesicles; black arrows, liver sinusoidal fenestrae; and white arrows, liver sinusoidal endothelial cells. Scale bars, 2 μm (main images) and 500 nm (magnified images). **(B-C)** Representative immunofluorescence images of the liver and colon stained for CD31 and α-smooth muscle actin (α-SMA) (B) or CD31 and ZO-1 (C), with quantification of α-SMA$^+$ or ZO-1$^+$ areas relative to the CD31$^+$ vascular area (n = 4 per group). Scale bars, 100 μm. **(D-F)** Representative three-dimensional reconstructions of CD31$^+$ vascular networks in the bone marrow (D), liver (E), and colon (F), acquired by light-sheet fluorescence microscopy after in vivo labeling with an anti-CD31 antibody. Upper panels show CD31$^+$ vasculature; lower panels show the corresponding computational vascular models, pseudo colored to indicate vascular branching levels (green, lower; red, higher). Scale bars,150 μm. **(G)** Descriptive whole-specimen measurements of CD31$^+$ vascular networks in the colon, liver, and bone marrow from syngeneic and aGVHD recipients. Vascular volume density (VVD), vascular length density (VLD), and branch density are listed for each organ and group. **(H)** Representative higher-magnification images of CD31$^+$ vasculature in the colon, liver, and bone marrow. **(I)** Evans blue extravasation in the liver and colon, expressed as nanograms of Evans blue per milligram of tissue (n = 5 per group). Scale bars, 50 um. Data are presented as mean ± SEM and are from two experiments. P values were calculated using unpaired two-tailed Student t tests (B, C and I). *$P < .05$; **$P < .01$; ***$P < .001$.

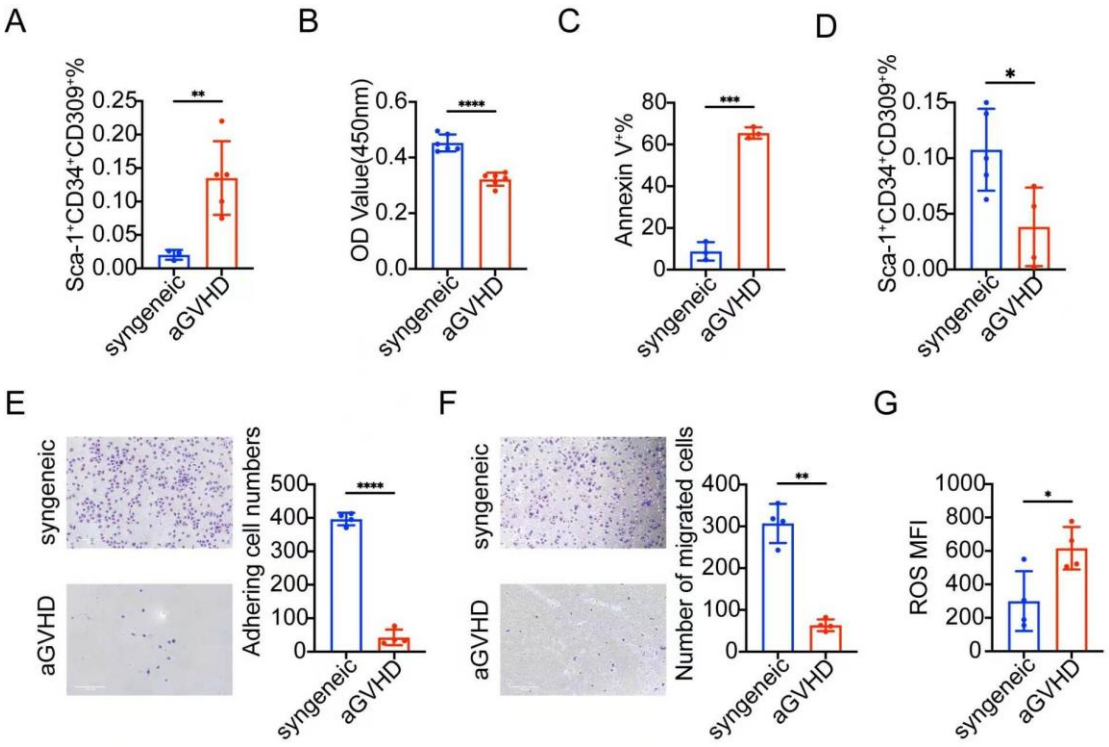

742

743 **Figure 3. aGVHD is associated with functional impairment of bone marrow-derived EPCs.**

744 Lethally irradiated BALB/c recipients were transplanted with bone marrow cells and splenocytes
745 from C57BL/6 donors as described in Figure 1. EPCs isolated from the bone marrow of aGVHD
746 recipients on day 15 after HSCT and cultured for 7 days in vitro. **(A)** Frequency of bone marrow
747 EPCs identified as Sca-1$^+$CD34$^+$CD309$^+$ cells by flow cytometry (n = 3-5 per group). **(B-C)**
748 CCK-8 activity, measured as absorbance at 450 nm (B), and apoptosis, assessed by Annexin
749 V/propidium iodide staining and expressed as the percentage of Annexin V$^+$ cells (C), n = 3-6 per
750 group. **(D)** Frequency of bone marrow Sca-1$^+$CD34$^+$CD309$^+$ EPCs on day 21 after HSCT (n = 4-5
751 per group). **(E-F)** Representative images and quantification of EPC adhesion (E) and Transwell
752 migration (F), n = 4 per group. **(G)** Intracellular ROS levels in EPCs, mean fluorescence intensity
753 (MFI) are shown, n = 4 per group. Data are presented as mean ± SEM and are from two
754 experiments. P values were calculated using unpaired two-tailed Student t tests. **P* < .05; ***P*
755 < .01; ****P* < .001; *****P* < .0001.

756

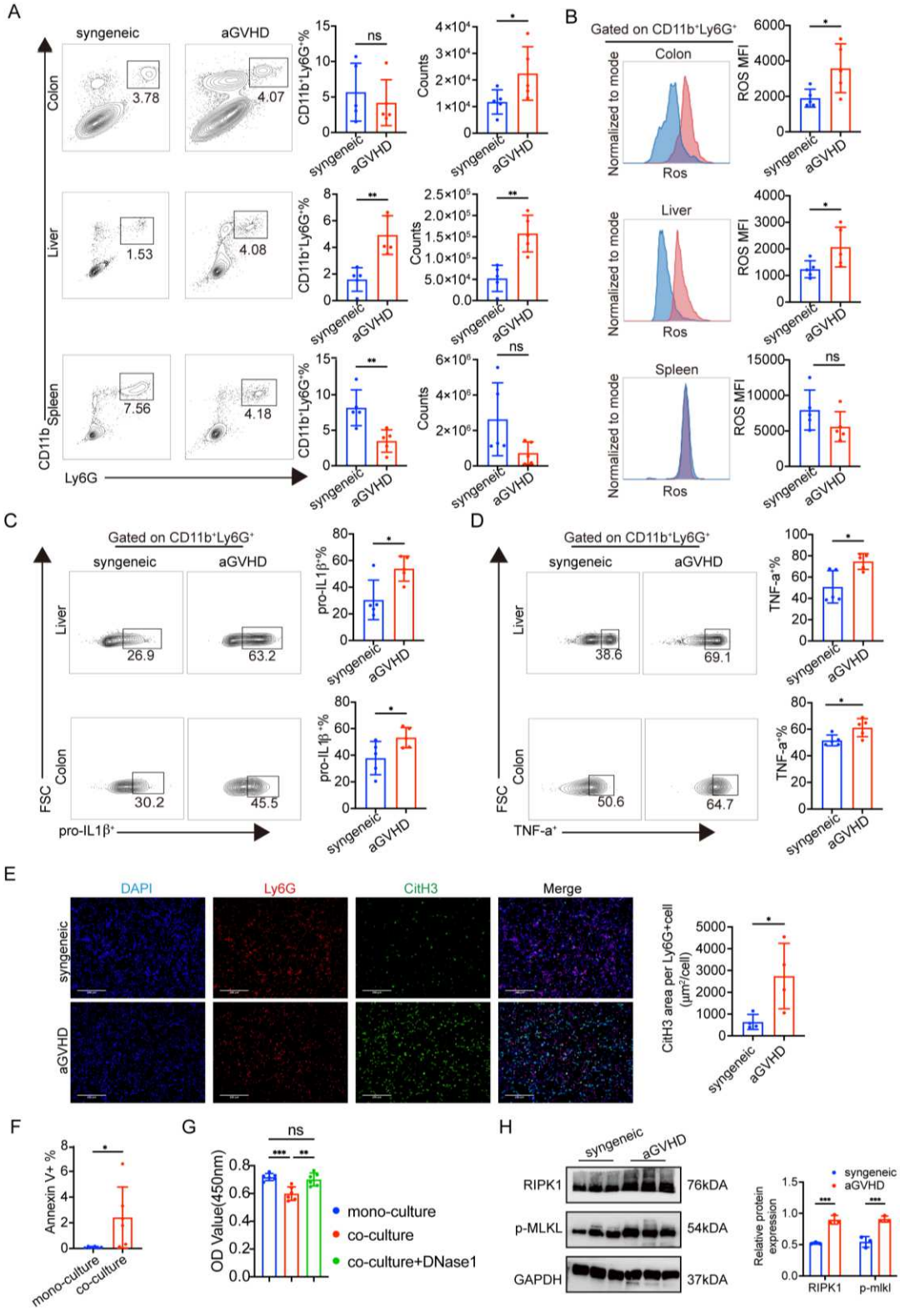
A
syngeneic
aGVHD
Colon
Liver
Spleen
CD11b
Ly6G
3.78
4.07
1.53
4.08
7.56
4.18
CD11b+Ly6G+%
Counts
ns
B
Gated on CD11b+Ly6G+
Normalized to mode
Ros
ROS MFI
C
Gated on CD11b+Ly6G+
FSC
pro-IL1β+
26.9
63.2
30.2
45.5
pro-IL1β+%
D
TNF-a+
38.6
69.1
50.6
64.7
TNF-a+%
E
DAPI
Ly6G
CitH3
Merge
CitH3 area per Ly6G+cell (μm²/cell)
F
Annexin V+ %
mono-culture
co-culture
G
OD Value(450nm)
co-culture+DNase1
H
RIPK1
p-MLKL
GAPDH
76kDA
54kDA
37kDA
Relative protein expression
p-mlkl

757

Figure 4. Donor-derived neutrophil mediates EPC apoptosis and is associated with activation of RIPK1 signaling. aGVHD and syngeneic control mice were generated as described in Figure 1. Tissues were collected on day 15. **(A)** Representative flow cytometry plots and quantification of $CD11b^+Ly6G^+$ neutrophil frequencies and absolute numbers in the colon, liver, and spleen (n = 5). **(B)** Representative flow cytometry histograms and quantification of intracellular ROS in $CD11b^+Ly6G^+$ neutrophils from the colon, liver, and spleen, expressed as mean fluorescence intensity (MFI; n = 5). **(C-D)** Representative flow cytometry plots and percentages of pro-IL-$1\beta^+$ (C) and TNF-α^+ (D) cells among $CD11b^+Ly6G^+$ neutrophils in the liver and colon (n = 5). **(E)** Representative immunofluorescence images of bone marrow neutrophils stained for Ly6G (red), citrullinated histone H3 (CitH3; green), and DNA (DAPI; blue), with quantification of $CitH3^+$ area normalized to the number of $Ly6G^+$ cells (μm^2/cell; n = 4). Scale bars, 200 μm. **(F-G)** Bone marrow-derived EPCs from wild-type C57BL/6 mice were cultured alone or cocultured with bone marrow neutrophils from aGVHD recipients at an EPC-to-neutrophil ratio of 1:20 for 6 hours, n=6. **(F)** The percentage of Annexin V^+ EPCs. **(G)** CCK-8 absorbance at 450 nm in EPC monoculture, EPC-neutrophil coculture, and coculture supplemented with DNase I (25 U/ml), added at the start of coculture. **(H)** Representative immunoblots and densitometric quantification of RIPK1 and p-MLKL in EPCs from syngeneic and aGVHD recipients, normalized to GAPDH (n = 3). Data are presented as mean ± SEM and pooled from two independent experiments. Statistical significance was assessed using unpaired two-tailed Student t tests (neutrophil frequencies in A; C-F and H), Mann-Whitney U tests (absolute neutrophil numbers in A and ROS levels in B), or one-way ANOVA (G). ns, not significant; *P <0 .05; **P < 0.01; ***P < 0.001; ****P < 0.0001.

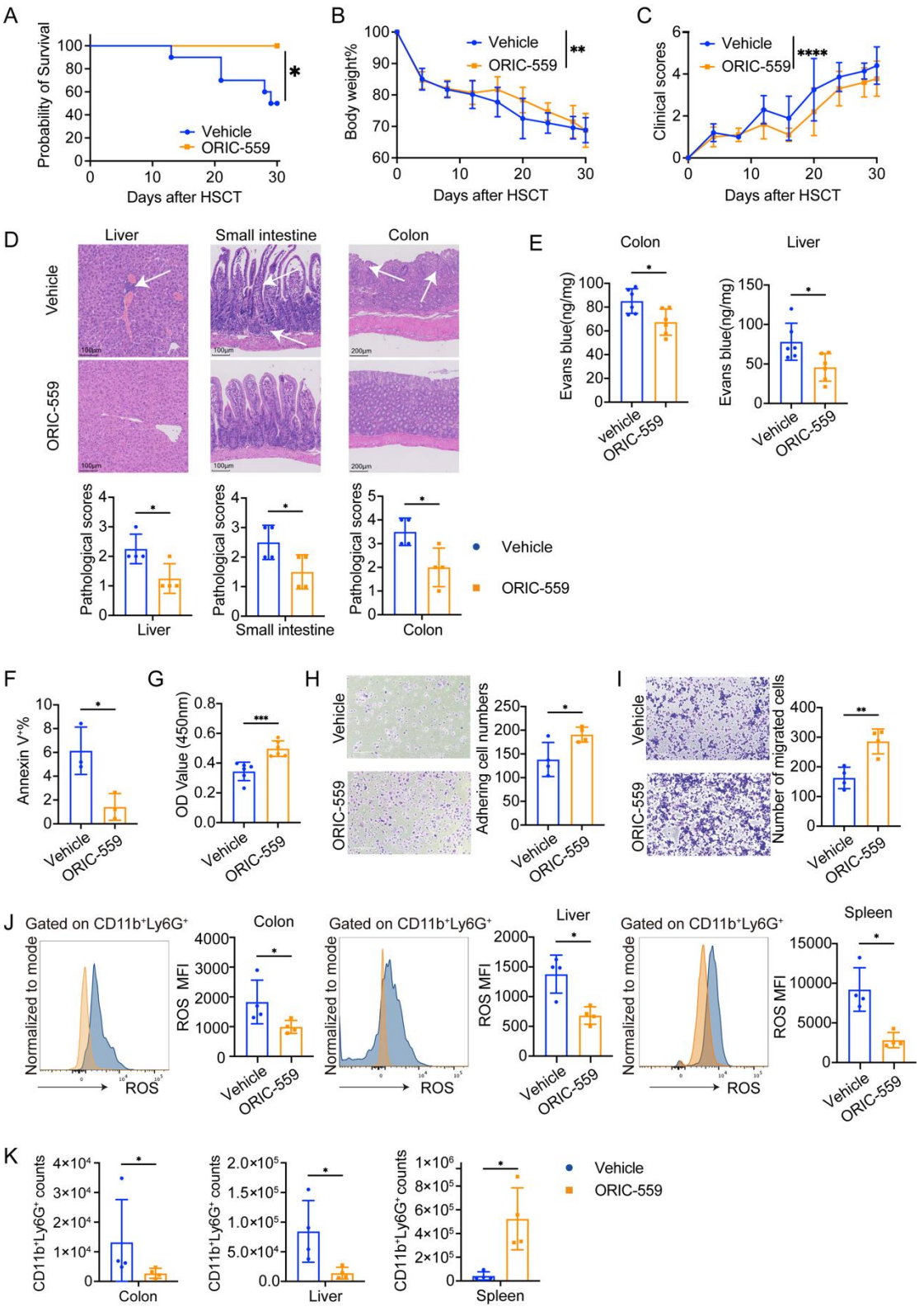

781

782 **Figure 5. Pharmacologic RIPK1 inhibition improves EPC function and attenuates aGVHD.**

783 aGVHD was induced as described in Figure 1. Beginning on day 7 after HSCT, recipients

received ORIC-559 (40 mg/kg) or vehicle twice daily by oral gavage. **(A-C)** Survival **(A)**, body weight change **(B)**, and clinical aGVHD scores **(C)** after HSCT (n = 10 per group). **(D)** Representative H&E-stained sections of the liver, small intestine, and colon on day 20 after HSCT, with corresponding histopathologic scores (n = 4 per group). Arrows indicate representative areas of inflammatory infiltration or mucosal injury. Scale bars, 100 μm (liver and small intestine) and 200 μm (colon). **(E)** Evans blue extravasation in the colon and liver on day 20, nanograms of Evans blue per milligram of tissue are shown (n = 6 per group). **(F-I)** EPCs were isolated from bone marrow on day 20 and cultured for 7 days (n = 3-6 per group). CCK-8 absorbance was corrected by subtracting the background signal from medium containing CCK-8 reagent without cells. Percentage of Annexin V^+ cells are shown **(F)**, and CCK-8 absorbance at 450 nm **(G)**. Representative images and quantification of EPC adhesion **(H)** and Transwell migration **(I)**. **(J-K)** On day 20 after HSCT, spleen, liver and colon were collected for flow cytometry analysis, n=4. Representative flow cytometry histograms and quantification of intracellular ROS in $CD11b^+Ly6G^+$ neutrophils from the colon, liver, and spleen, mean fluorescence intensity (MFI) are shown **(J)**. Absolute numbers of $CD11b^+Ly6G^+$ neutrophils in the colon, liver, and spleen **(K)**. Data are presented as mean ± SEM and are from 2-3 independent experiments. Statistical significance was assessed using the log-rank test (A), two-way ANOVA (B-C), unpaired two-tailed Student t tests (D-I), or Mann-Whitney U tests (J-K). $*P < 0.05$; $**P < 0.01$; $***P < 0.001$; $****P < 0.0001$.

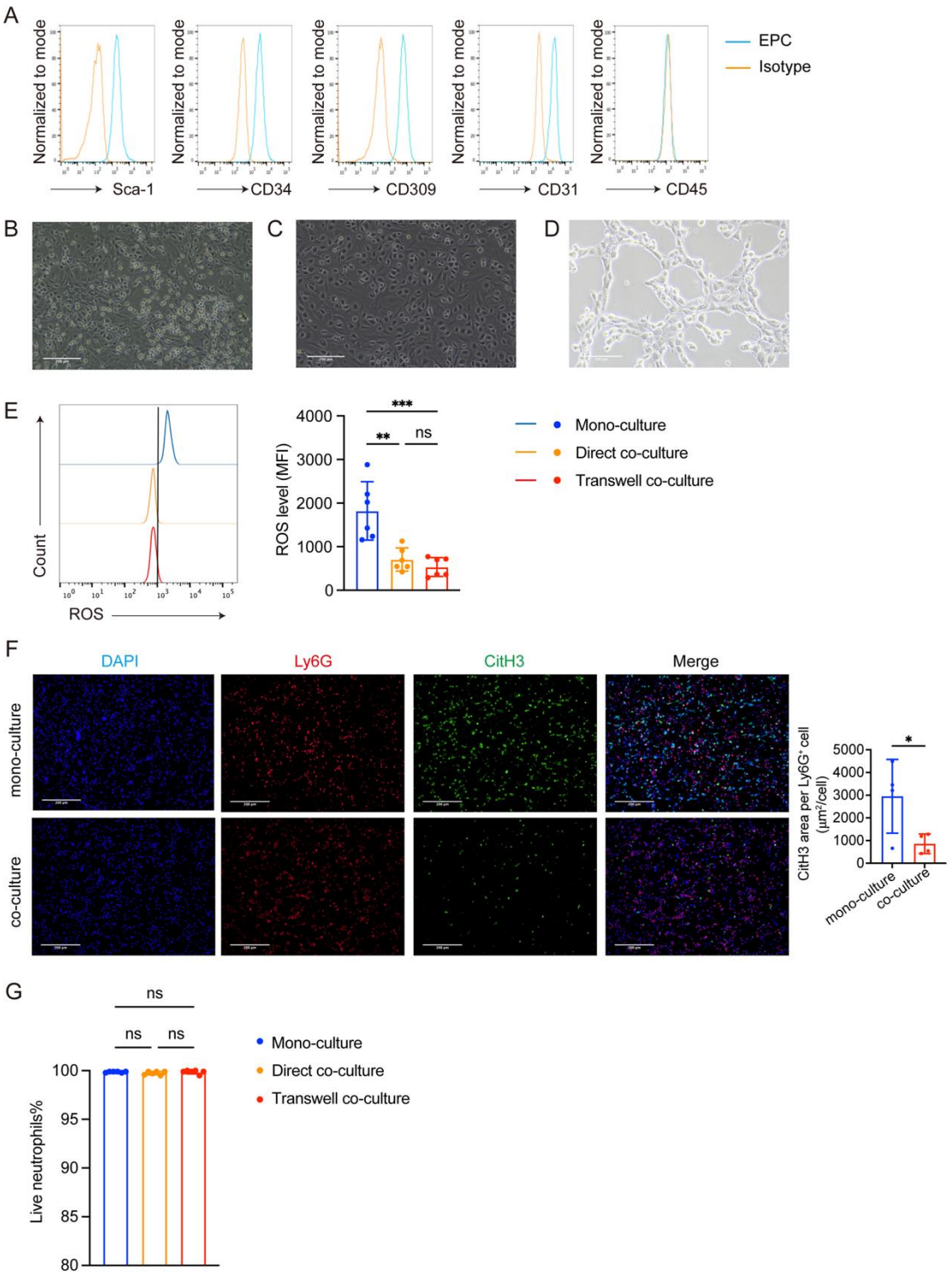

804

805 **Figure 6. Ex vivo-expanded EPCs suppress neutrophil oxidative activity and NETs**
806 **formation. (A)** Representative flow cytometry histograms showing Sca-1, CD34, CD309, CD31,
807 and CD45 staining in ex vivo-expanded bone marrow-derived EPCs. Blue, EPCs stained with

marker-specific antibodies; orange, isotype controls. **(B-C)** Representative phase-contrast images of EPC cultures at passage 0 (P0; B) and passage 1 (P1; C). Scale bars, 200 μm. **(D)** R Representative image of capillary-like networks formed by EPCs on Matrigel. Scale bar, 100 μm. **(E-G)** Bone marrow neutrophils isolated from aGVHD recipients were cultured alone (monoculture), in direct contact with EPCs (direct coculture), or separated from EPCs by a Transwell membrane (Transwell coculture), as indicated. Cocultures were maintained at an EPC-to-neutrophil ratio of 1:1 for 4 hours. **(E)** Representative flow cytometry histograms and quantification of intracellular ROS in $CD11b^{+}Ly6G^{+}$ neutrophils, assessed by DCFH-DA staining and expressed as mean fluorescence intensity (MFI; n = 6 per group). **(F)** Representative immunofluorescence images of neutrophils cultured alone or directly cocultured with EPCs, stained for DNA (DAPI; blue), Ly6G (red), and citrullinated histone H3 (CitH3; green). $CitH3^{+}$ area was normalized to the number of $Ly6G^{+}$ cells and expressed as μm^2/cell (n = 4 per group). Scale bars, 200 μm. **(G)** Neutrophil viability under the three culture conditions is described in E (n = 6 per group). Data are presented as mean ± SEM and are representative of three independent experiments. Statistical significance was assessed using one-way ANOVA with multiple comparisons (E and G) or an unpaired two-tailed Student t test (F). ns, not significant; $*P < 0.05$; $**P < 0.01$; $***P < 0.001$.

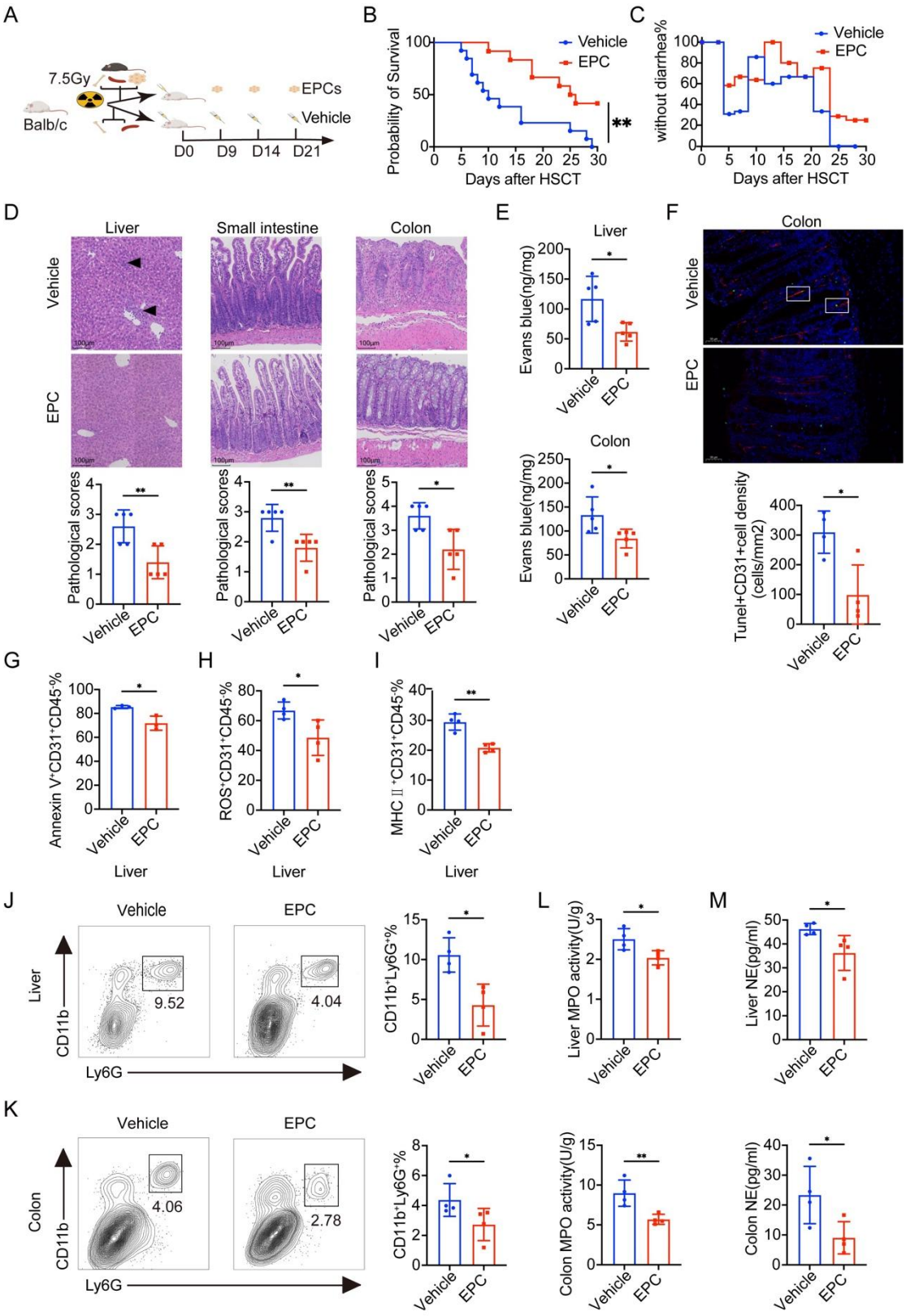
A
7.5Gy
Balb/c
EPCs
Vehicle
D0
D9
D14
D21
B
Probability of Survival
Vehicle
EPC
**
Days after HSCT
C
without diarrhea%
Vehicle
EPC
Days after HSCT
D
Liver
Small intestine
Colon
Vehicle
EPC
Pathological scores
E
Liver
Evans blue(ng/mg)
Colon
F
Colon
Tunel+CD31+cell density (cells/mm2)
G
Annexin V+CD31+CD45-%
H
ROS+CD31+CD45-%
I
MHC II +CD31+CD45-%
J
Vehicle
EPC
Liver
CD11b
Ly6G
9.52
4.04
CD11b+Ly6G+%
L
Liver MPO activity(U/g)
M
Liver NE(pg/ml)
K
Colon
4.06
2.78
Colon MPO activity(U/g)
Colon NE(pg/ml)

826

Figure 7. EPC administration attenuates aGVHD and reduces vascular injury. aGVHD recipients received EPCs (1×10^6 cells per mouse per injection) or PBS according to the administration schedule on panel A. Tissue analyses were performed on day 15. **(A)** Schematic of aGVHD induction and the EPC administration schedule. **(B-C)** Survival (B) and the percentage of mice without diarrhea at each assessed time point (C; n = 12-13 per group). **(D)** Representative H&E-stained sections of the liver, small intestine, and colon, with corresponding histopathologic scores (n = 5 per group). Arrows indicate representative areas of hepatic inflammatory infiltration. Scale bars, 100 μm. **(E)** Evans blue extravasation in the liver and colon, nanograms of Evans blue per milligram of tissue are shown (n = 5 per group). **(F)** Representative immunofluorescence images of colon sections stained for CD31 and TUNEL, with DAPI counterstaining. $TUNEL^+CD31^+$ cell density was quantified as the number of double-positive cells per mm^2 of $CD31^+$ area (n = 4 per group). Scale bars, 50 μm. **(G-I)** Flow cytometry quantification of Annexin V^+ (G), ROS^+ (H), and MHC class II^+ (I) cells among hepatic $CD45^-CD31^+$ endothelial cells (n = 3-4 per group). Intracellular ROS was assessed using DCFH-DA staining. **(J-K)** Representative flow cytometry plots and frequencies of $CD11b^+Ly6G^+$ neutrophils in the liver (J) and colon (K); n = 4 per group. **(L)** MPO activity in the liver and colon, units per gram of tissue are shown (U/g); n = 4 per group. **(M)** NE concentrations in the liver and colon, measured by ELISA and showed as pg/ml (n = 4 per group). Data are presented as mean ± SEM and pooled from 2-3 independent experiments. Statistical significance was assessed using the log-rank test (B) or unpaired two-tailed Student t tests (D-M). $*P < 0.05$; $**P < 0.01$.

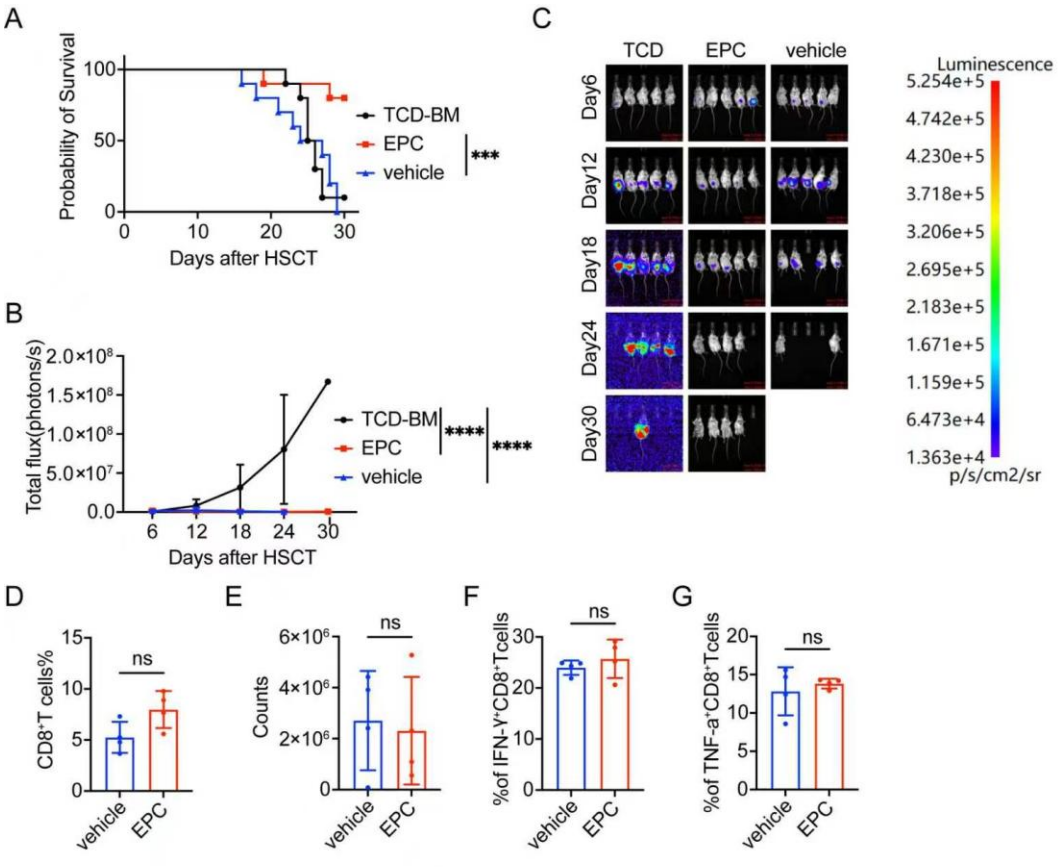

Figure 8. EPC administration improves survival while preserving GVL activity. The GVL model was established as described in the Methods. Lethally irradiated BALB/c recipients received luciferase-expressing A20 lymphoma cells and C57BL/6 T cell-depleted bone marrow (TCD-BM), either without donor splenocytes (TCD-BM group) or with donor splenocytes (vehicle and EPC groups). The EPC group received EPCs (1×10^6 cells per mouse per injection) on days 0, 9, 14, and 21 after HSCT; control groups received PBS. **(A)** Overall survival after HSCT (n = 10 per group). **(B)** Longitudinal quantification of leukemia-associated bioluminescence, showed as total photon flux (photons/s; initial n = 10 per group). **(C)** Representative in vivo bioluminescence images on days 6, 12, 18, 24, and 30 after HSCT, acquired using an Aniview 600 imaging system. **(D-E)** Frequency (D) and absolute number (E) of splenic $CD8^+$ T cells on day 15 after HSCT in vehicle- and EPC-treated recipients, assessed by flow cytometry (n = 4). **(F-G)** Percentages of IFN-γ^+ (F) and TNF-α^+ (G) cells among splenic

861 $CD8^+$ T cells on day 15 after HSCT, assessed by flow cytometry (n = 4). Data are presented as
862 mean ± SEM and pooled from 2-3 independent experiments. Statistical significance was assessed
863 using the log-rank test (A), two-way ANOVA (B), or unpaired two-tailed Student t tests (D-G).
864 ns, not significant; ***$P < 0.001$; ****$P < 0.0001$.

Supplementary Files

This is a list of supplementary files associated with this preprint. Click to download.

- video1.mov
- video2.mov
- video3.mov